KeAi
CHINESE ROOTS
GLOBAL IMPACT

Contents lists available at ScienceDirect

### Petroleum Science

journal homepage: www.keaipublishing.com/en/journals/petroleum-science



### Original Paper

# The influence mechanism of liquid sedimentary layers in urban underground spaces on the characteristics of natural gas explosions and damage risk



Qi Jing <sup>a, b</sup>, Zi-Yu Fan <sup>a, b</sup>, Rui Zhou <sup>a, b</sup>, Yun-Tao Li <sup>a, b, \*</sup>

- <sup>a</sup> College of Safety and Ocean Engineering, China University of Petroleum (Beijing), Beijing, 102249, China
- <sup>b</sup> Key Laboratory of Oil and Gas Safety and Emergency Technology, Ministry of Emergency Management, Beijing, 102249, China

#### ARTICLE INFO

#### Article history: Received 30 October 2024 Received in revised form 2 January 2025 Accepted 12 March 2025 Available online 14 March 2025

Edited by Min Li

Keywords: Underground space Liquid fullness degree Gas-liquid coexistence Peak overpressure Explosive risk

### ABSTRACT

Gas explosions are a frequent hazard in underground confined spaces in the process of urban development. Liquid sedimentary layers, commonly present in these environments, have not been sufficiently studied in terms of their impact on explosion dynamics. This study aims to investigate how gas-liquid two-phase environments in confined underground spaces affect the explosion characteristics of natural gas. To achieve this, experiments are conducted to examine the propagation of natural gas explosions in water and diesel layers, focusing on the influence of liquid properties and the liquid fullness degree  $(L_x)$  on explosion behavior. The results indicate that the presence of a liquid layer after the initial ignition stage significantly attenuates both the peak overpressure and the rise speed of pressure, in comparison to the natural gas conditions. During the subsequent explosive reaction, the evaporation and combustion of the diesel surface resulted in a distinct double-peak pressure rise profile in the diesel layer, with the second peak notably exceeding the first peak. Under conditions with a liquid sedimentary layer, the flame propagation velocities range from 6.53 to 34.1 m/s, while the overpressure peaks vary between 0.157 and 0.255 MPa. The explosion duration in both the water and diesel layer environments is approximately twice as long as that of the natural gas explosion, although the underlying mechanisms differ. In the diesel layer, the prolonged explosion time is attributed to the evaporation and combustion of the diesel, while in the water layer, the flame propagation velocity is significantly reduced. Under the experimental conditions, the maximum explosion energy reached 7.15 imes  $10^6$  J, corresponding to a TNT equivalent of 1.7. The peak overpressure surpassed the threshold for human fatality as defined by overpressure standards, posing a potential risk of damage to large steel-frame structures. The explosion shockwave in diesel layer conditions ( $L_d = 0\%$ , 5%, 7.5%, 12.5%) and water layer ( $L_w = 12.5\%$ ) conditions is observed to be sufficient to damage earthquake-resistant reinforced concrete. This study investigates the impact of sediment layer thickness and composition on gas explosions, and evaluates the associated explosion energy to assess human injuries and structural damage in underground environments. The findings of this study provide a scientific reference for urban underground safety.

© 2025 The Authors. Publishing services by Elsevier B.V. on behalf of KeAi Communications Co. Ltd. This is an open access article under the CC BY license (http://creativecommons.org/licenses/by/4.0/).

### 1. Introduction

As shown in Fig. 1, during urban development, long-distance oil and gas pipelines, various municipal networks, and schools, residential areas, and major transportation routes are intertwined. In the event of corrosion or construction damage, leaking oil and gas can directly enter underground spaces, forming a complex environment with a lower layer of liquid accumulation and an upper

\* Corresponding author.

E-mail address: liyt@cup.edu.cn (Y.-T. Li).

layer of combustible gases within the underground space (Chen et al., 2016; Li et al., 2021; Zhao et al., 2024). Explosions caused by ignition sources are common in such environments, leading to severe casualties, property damage, and environmental contamination (Lee et al., 2021; Li et al., 2023; Xu et al., 2020; Zhang et al., 2023). Therefore, studying the impact mechanisms of liquid accumulation on gas explosions is of practical significance for enhancing urban underground safety.

Currently, both domestic and international scholars have conducted extensive research on gas explosions in confined spaces (He et al., 2022; Lu et al., 2024; Zhou et al., 2023), focusing on the properties of gas ignition sources, explosion process dynamics

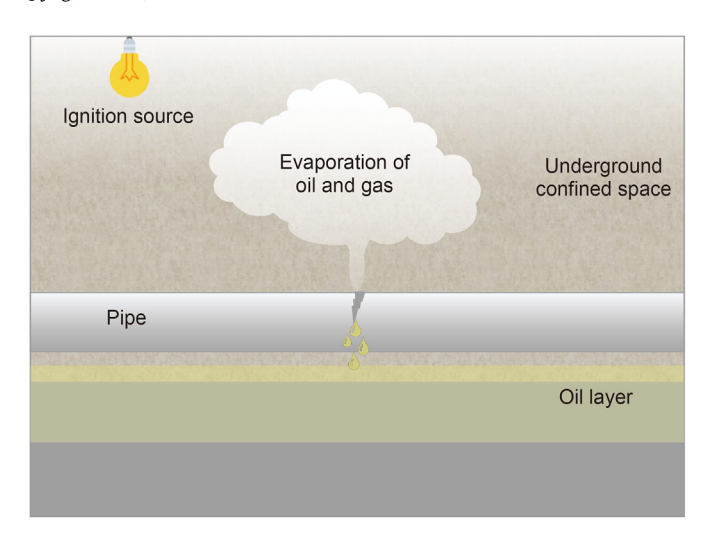


Fig. 1. Schematic diagram of the accident.

(Shen et al., 2022), flame acceleration mechanisms (Xiao et al., 2010), and the impact of obstacle distribution within the space on the explosion process (Yang et al., 2024c). Pang et al. (2025) and Yang et al. (2024a, 2024b) investigated the effect of gas concentration distribution on explosion characteristics, revealing that variations in gas mixture concentration significantly influence explosion overpressure and flame velocity. Yu et al. (2024) carried out an experimental study on methane-air mixtures using a closed pipe to investigate the effect of methane concentration on explosion characteristics. Guo et al. (2024) performed premixed gas/air explosion experiments in parallel narrow channels, analyzing flame propagation, explosion overpressure, and temperature in confined spaces. Qi et al. (2024) conducted hydrogen-rich natural gas explosion experiments in a closed pipeline, analyzed the effect of hydrogen content on natural gas flame propagation, flame stability and explosion intensity, and revealed the premixed flame structure and combustion mechanism of hydrogen-natural gas mixtures.

Additionally, numerous studies have examined gas explosions in confined spaces under conditions involving liquid phases. Notably, Zhao et al. (2001) investigated the attenuation of explosive waves in the presence of water through numerical simulations, analyzing the effects of liquid media on gas explosion limits, flame propagation, overpressure characteristics, and energy conversion. Feng et al. (2024) explored the diffusion and mixing characteristics of kerosene affected by evaporation under shock wave conditions, focusing on the influence patterns and enhancement mechanisms of shock waves on kerosene diffusion and mixing capabilities. Sugiyama et al. (2016) used numerical simulations to model explosions in water-saturated L-shaped tunnels, investigating the attenuation effect of internal energy transfer at the water-air interface on shock waves. Their results demonstrated a significant reduction in peak overpressure in water-saturated environments. Nowak et al. (2023) conducted small-scale underwater explosion experiments in a shallow water tank, obtaining pressure propagation processes in aqueous media and analyzing the behavior of shock waves reflected from the tank bottom, surface, and vertical walls. Wang et al. (2021) investigated the explosion characteristics of methane under multi-phase conditions, discovering that in a slender pipe with a volume of 76 L, the flammability limits of the gas exhibit a volumetric effect, with pure methane's flammability limit ranging from 9% to 17%. Zhang et al. (2020) performed numerical simulations of methane explosions ignited by electrical sparks in a pipeline with a water environment, analyzing flame propagation patterns under both wet and dry conditions. Lv et al.

(2021) used a custom-designed explosion test pipeline to conduct comparative experiments under varying water fullness degrees and methane concentrations, exploring the dual effects of water storage on methane deflagration pressure suppression and enhancement. They found that water storage could reduce the methane deflagration temperature, prolong the time to reach the deflagration peak temperature, alter the shape of the methane deflagration flame front, and reduce the flame propagation velocity.

Recent studies on gas explosions involving liquid layers have primarily concentrated on the impact of water layers on explosion process. However, limited research has been conducted on the effects of continuous liquid phases such as oil layers, on the propagation characteristics of natural gas explosions. Most studies have been restricted to water layers, with a lack of research on oil layer accident scenes, and the mass and heat transfer characteristics between gas explosions and liquid phases remain unexplored. Therefore, this study has developed a gas explosion pipeline experimental system that can accommodate different liquids. Utilizing a range of monitoring techniques including optical, pressure, and electrical methods, the research varies the volume and type of liquid to investigate the effects of liquid phase properties and liquid fullness degree on the flame propagation and pressure characteristics of natural gas explosions. The findings are expected to provide a theoretical basis for improving urban underground safety levels.

### 2. Experimental methodology

A gas explosion pipeline experimental system capable of accommodating liquids is constructed. The main components of the experimental platform include a pipeline system, a gas supply system, an ignition system, a multi-channel data acquisition system, a synchronized trigger system, and a liquid injection and a waste liquid collection system. The experiments are conducted in a metal pipeline with a certain compressive strength, with a length-to-diameter ratio of 27.5. Sensors are placed at different positions along the pipeline to measure the relevant optical, electrical, and pressure data when the explosion propagates to those locations.

The study simulated accident scenes involving the leakage of natural gas and oil into adjacent confined underground spaces, such as sewage pipes. The experimental pipeline is 3000 mm in total length, consisting of three 1000 mm-long segments connected in series by flange seals. The central segment contains symmetrically arranged observation windows constructed from 20 mm thick hard quartz glass, each measuring 366 mm by 80 mm, as shown in Fig. 2. The pipeline has an inner diameter of 109 mm, and an outer diameter of 133 mm, with a pressure tolerance exceeding 6 MPa to ensure safety during experiments. One end of the pipeline is connected to the gas supply system and liquid injection system, while the other end is connected to the ignition system and waste liquid collection system. The ignition system is an oscillatory electrical spark discharge apparatus (model KTGD-B) manufactured by Shaanxi Kehui Thermal Technology Co., Ltd. This device features a spark needle diameter of 2 mm, a discharge gap of 1 mm, an ignition duration of 300 ms, a control voltage of 150 V, and an effective ignition energy of 2 J.

The gas supply system serves three primary functions: evacuating the pipeline, preparing the mixed gas, and removing exhaust gases. The gas distribution unit is connected to high-pressure natural gas cylinders, ambient air, a vacuum pump, and fume hoods. The natural gas is prepared according to the national urban gas network specifications, with a composition of methane (93.221%), ethane (4.175%), propane (1.629%), *n*-butane (0.42%), isobutane (0.394%), pentane (0.024%), and nitrogen (0.137%).The circulation system consists of sealed rubber hoses (inner diameter 8 mm) that are connected to both ends of the pipeline, with an

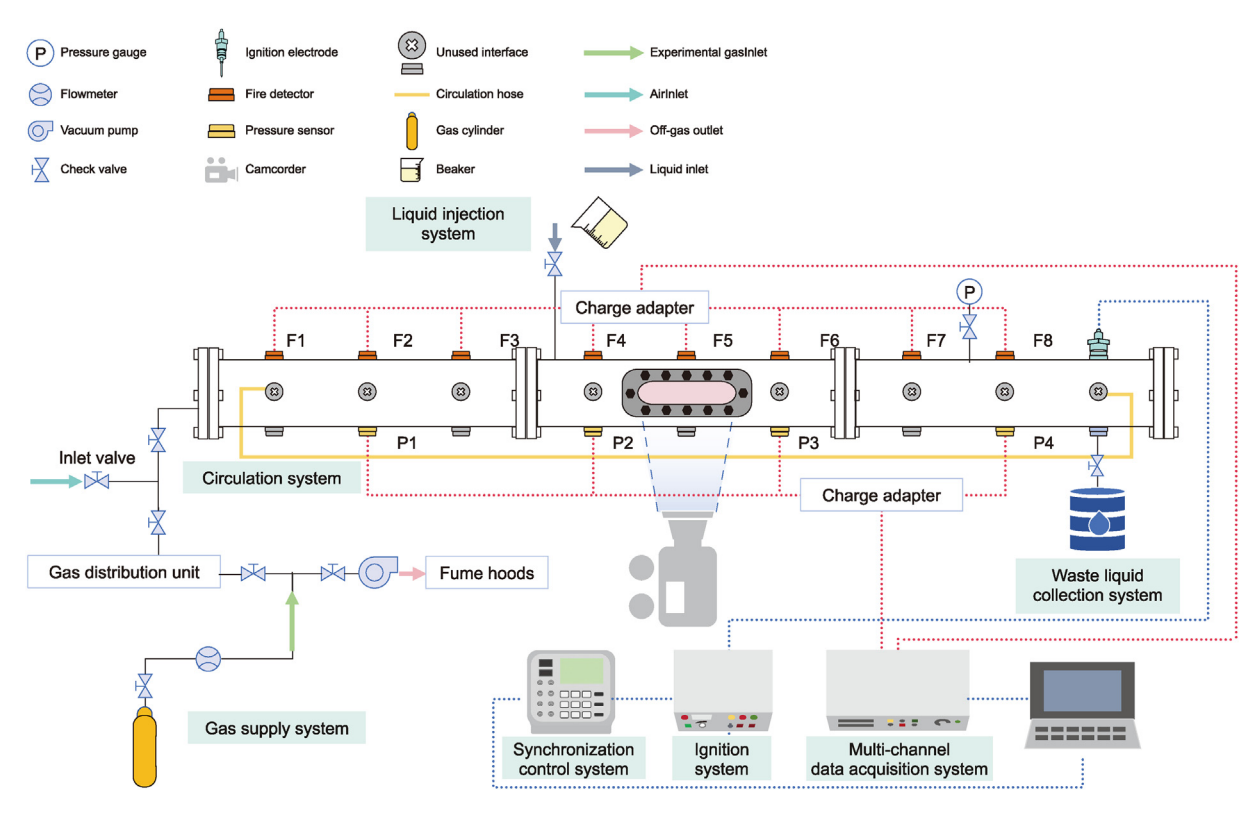


Fig. 2. Schematic diagram of the experimental system.

explosion-proof circulation fan placed in the middle, which is designed to accelerate the uniform mixing of multi-component gases within the pipeline. The multi-channel data acquisition system includes a piezoresistive pressure sensor (Baoji Zhixing Sensor Co., Ltd., model ZXP611, range 0–1 MPa, accuracy 0.25% FS), a high-precision fire detector (Hamamatsu Photonics, model R2868, response time 1  $\mu s$ ), and a DHDAS dynamic signal acquisition and analysis device (Jiangsu Donghua Testing Technology Co., Ltd., model DH8301, sampling frequency 1 MHz). The synchronization control system uses an NH-1315 digital pulse delay blaster (Chengdu Nanhui Technology Co., Ltd., pulse width time 1–3000 ms) to precisely control the start and stop times of each subsystem. The installation coordinates of the pressure sensors (P1–P4) and fire detectors (F1–F8) are listed in Table 1.

The liquid injection system manages the addition of the liquid medium, whereas the waste liquid collection system handles its discharge. The liquid injection system is equipped with a fine tube connected above the midpoint of the pipeline, while the waste liquid collection system features a collection vessel located below the end of the pipeline. During the experiment, the required volume of liquid is calculated based on the designed liquid fullness degree for each working condition and is injected into the pipeline via the fine tube. Waste liquid generated during the experiment is collected and processed by laboratory waste management personnel to prevent environmental pollution.

The liquid fullness degree ( $L_x$ ), defined as the ratio of liquid volume to pipeline volume, is denoted as  $L_d$  for diesel and  $L_w$  for water, as illustrated in Fig. 3. In this study,  $L_x$  was precisely controlled by calculating the required liquid volume based on the pipe's dimensions. A calibrated syringe was employed to ensure accurate injection and minimize measurement errors.

$$V_{\rm p} = l_0 \times \pi \times r^2 \tag{1}$$

$$V_{\rm x} = l_0 \times \left[ \alpha \times r^2 - r \times (r - h) \times \sin \alpha \right]$$
 (2)

$$L_{\rm X} = \frac{V_{\rm X}}{V_{\rm D}} \tag{3}$$

where  $V_x$  represents the liquid volume in cm<sup>3</sup>,  $V_p$  represents the pipeline volume in cm<sup>3</sup>, and  $l_0$  is the length of the experimental pipeline, 3000 mm.

This paper investigates the explosion characteristics of natural gas in different liquid deposit layers. The natural gas condition is defined as the scene where the experimental pipeline contains only a natural gas-air mixture with an equivalence ratio of 1.0 and  $L_{\rm x}$  is 0%. The other 10 scenes involve injecting two types of liquid component (water  $L_{\rm w}$  and diesel  $L_{\rm d}$ ) at five different liquid fullness degree (5%–15%) into the pipeline along with the combustible gas,

**Table 1** Sensor installation position coordinates.

Sensors	Coordinates, mm	Detectors	Coordinates, mm	Detectors	Coordinates, mm
P1	500	F1	500	F5	1834
P2	1167	F2	833.5	F6	2167.5
P3	1834	F3	1167	F7	2501
P4	2501	F4	1500.5	F8	2834.5

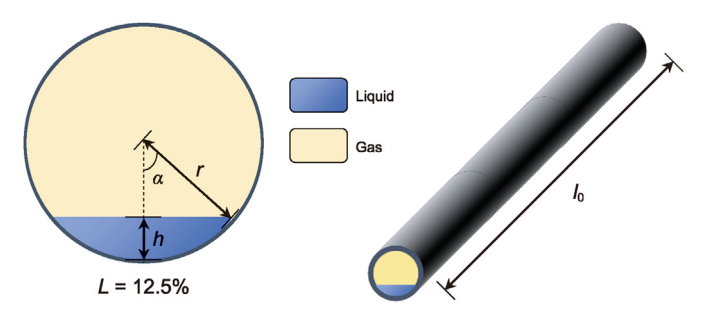


Fig. 3. Schematic diagram of liquid fullness degree.

in accordance with Dalton's law of partial pressures. The experimental conditions are detailed in Table 2. To ensure the validity and repeatability of the results, each experimental condition was repeated three times, and the average value is used for analysis. All instruments were calibrated, and environmental factors such as temperature and pressure were controlled to minimize their impact. Additionally, potential operational errors were minimized to ensure data consistency and accuracy.

### 3. Results and discussion

3.1. The effect of different liquid environments on the propagation pattern of natural gas explosions

# 3.1.1. Natural gas explosion propagation mechanisms in a natural gas environment

In the natural gas explosion experiment, the typical monitoring curves from four pressure sensors uniformly distributed along the pipeline are shown in Fig. 4. The overpressure curves at all four points exhibit similar trends and peak values, reflecting the uniformity of pressure changes along the pipeline. This consistency can be attributed to the slow progression of the natural gas-air mixture explosion under weak ignition conditions, which results in a relatively slow flame propagation velocity. The gas expansion and pressurization caused by heat conduction at the flame front generate compression waves propagating in both forward and backward directions. The propagation velocity of these compression waves is equal to the local sound velocity, which is significantly higher than the flame propagation velocity. Therefore, the overall pressure within the pipeline remains relatively uniform at any given time. A typical pressure wave curve exhibits a double-peak characteristic, with two distinct rising segments in the rate of pressure rise curve. The reason for this phenomenon is that after the natural gas-air mixture is ignited, the forward-propagating compression wave causes the combustion products to move forward, compressing the unburnt gas downstream. The flame's initial

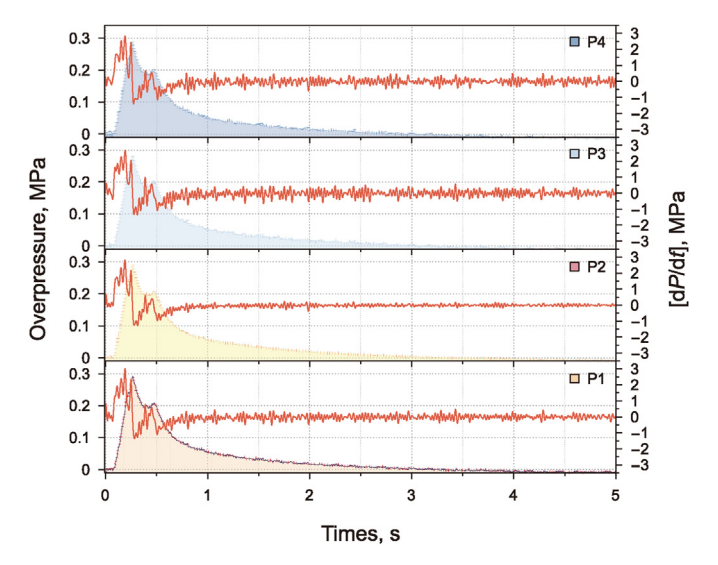


Fig. 4. Typical gas explosion overpressure wave curve characteristics.

forward-propagating heat release generates the first overpressure peak. Simultaneously, a significant amount of unreacted gas accumulates at the pipeline's end, where it oscillates with the reflected pressure wave. This unburned gas eventually undergoes complete combustion, leading to a pressure sub-peak and the formation of a second overpressure peak.

In the natural gas explosion experiment, a typical monitoring curves from eight sensitive fire detectors, uniformly distributed along the pipeline, are presented in Fig. 5. The flame take-off time of the response curve indicates the moment when the flame reaches the monitoring point, while the relative light intensity reflects the strength of the flame. It is evident that within the 0–1500 mm length range, the flame duration gradually decreases while the flame intensity increases. This suggests that the explosive reaction zone (ERZ) at the flame front narrows progressively, leading to a more concentrated energy release and an intensified flame. Beyond a distance of 1500 mm, the flame duration increases due to the oscillatory behavior of reflected pressure waves. In the 1500–3000 mm range, the flame front alternates between stretching and compressing, prolonging the explosion response time in this region.

Furthermore, by connecting the flame take-off times of each monitoring point, the propagation trajectory and velocity of the flame front can be determined, with specific values and patterns analyzed in subsequent sections. Analysis of the pressure waveform and flame intensity curves reveals that the pressure wave consists of rising and falling segments, with the effective explosive response sustained only between 0.09 and 0.63 s, encompassing the entire

Experimental conditions.

No.	Liquid components	Liquid fullness degree $L_x$ , %	Scene
1	-	-	Natural gas
2	Water	5.0	Natural gas-water layer
3	Water	7.5	Natural gas-water layer
4	Water	10.0	Natural gas-water layer
5	Water	12.5	Natural gas-water layer
6	Water	15.0	Natural gas-water layer
7	Diesel	5.0	Natural gas-diesel layer
8	Diesel	7.5	Natural gas-diesel layer
9	Diesel	10.0	Natural gas-diesel layer
10	Diesel	12.5	Natural gas-diesel layer
11	Diesel	15.0	Natural gas-diesel layer

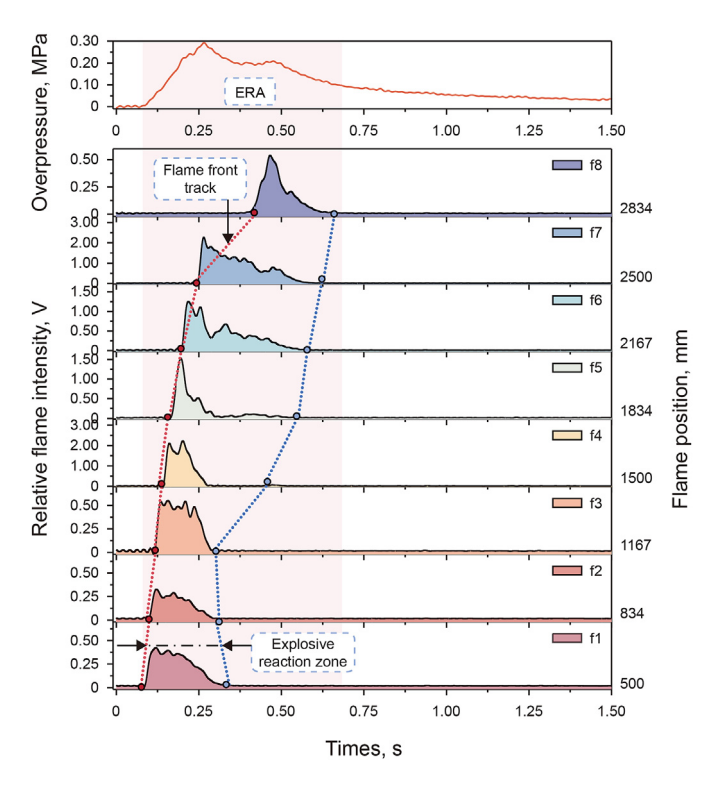


Fig. 5. Typical explosion flame propagation and reaction zone characteristics.

rising segment and part of the falling segment. Previous studies have generally regarded the peak of the pressure wave as indicative of the end of the explosive reaction, followed by a heat dissipation pressure relief phase. However, this study demonstrates that towards the end of the explosive reaction, the heat release rate is lower than the heat dissipation rate of the pipeline, resulting in a macroscopic pressure decrease while the explosive reaction has not yet completely ceased.

# 3.1.2. Natural gas explosion propagation mechanisms in a diesel layer environment

The pressure propagation characteristic curves from the natural gas-diesel layer explosion experiment are presented in Fig. 6. The pressure curves at the monitoring points indicate that the explosion overpressure curve, following the injection of diesel into the lower section of the pipeline, exhibits a bimodal characteristic analogous to that observed in natural gas explosion experiments. However, in contrast to the natural gas experiments, the peak overpressure in this set of experiments is significantly lower. Additionally, the second peak in the rate of pressure rise curve is significantly higher than the first peak. This phenomenon is attributed to the presence of diesel, which impedes both the forward propagation of the flame and the transmission of pressure waves during the initial ignition stage phase. Subsequently, the heat released by the propagating flame ignites the surface of the diesel layer, and the combustion of the diesel releases additional thermal energy. This energy promotes the oscillation of the pressure waves and sustains the reaction, resulting in a significant increase in the rate of pressure rise.

The flame propagation curves from the natural gas-diesel layer explosion experiments are shown in Fig. 7. Within the 0–1834 mm range, the flame duration decreases progressively while its increases. Beyond the 1834 mm, due to the oscillatory behavior of the reflected pressure waves, the flame duration increases. In the 1834–3000 mm range, the flame front alternates between

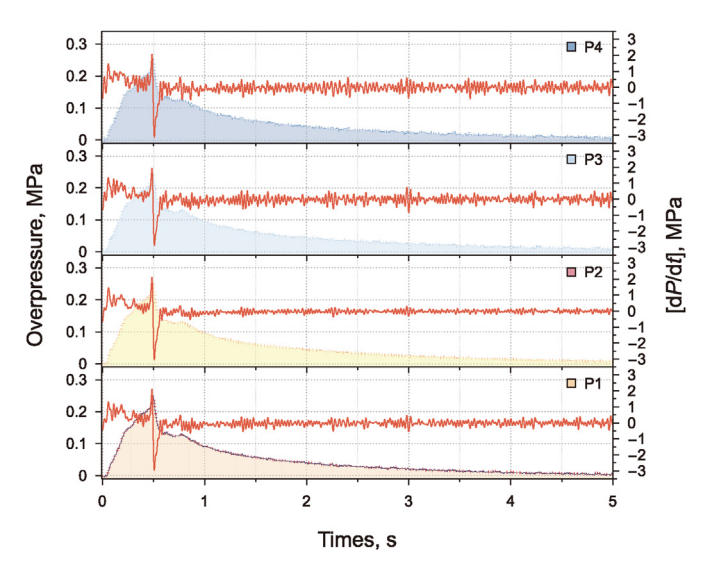
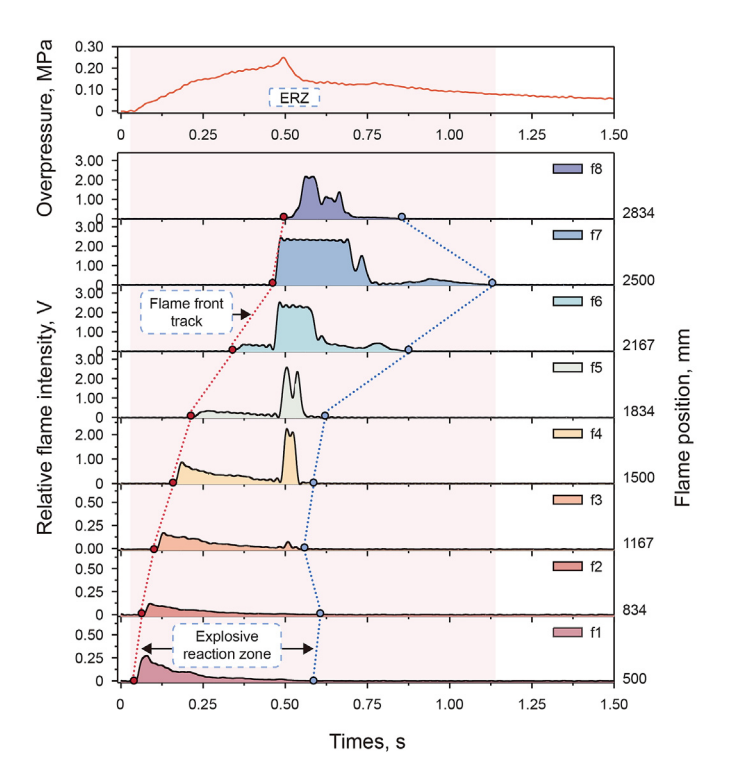


Fig. 6. Characteristics of gas explosion overpressure wave curve in diesel layer environment.

stretching and compressing, prolonging the explosive reaction in this region. With the addition of diesel, the space available for gas in the pipeline narrows, reducing the time required for the fireball to diffuse, which results in an earlier flame arrival time. The explosive reaction is sustained within the 0.047–1.13 s time range, representing a 100.56% increase in the explosion duration. This is because the combustion of diesel releases more energy, extending the flame's duration.

In this experiment, it is observed that the flame in the pipe continued to oscillate after its initial passage through the observation window. The oscillating flame appeared as a bright golden



**Fig. 7.** Typical flame propagation and reaction zone characteristics of a gas explosion in a diesel layer environment.

color, stronger than the initial red flame that first passed through the observation window. The explosion sound is sharp and crisp. This phenomenon occurred because the flame propagation increased the pressure and temperature inside the pipeline, igniting the liquid surface and releasing a large amount of heat energy.

## 3.1.3. Natural gas explosion propagation mechanisms in aquifer

In the natural gas-water layer explosion experiments, the overpressure peak values are significantly reduced, and no distinct peaks are observed in the rate of pressure rise curve, as shown in Fig. 8. This is because the water layer absorbs heat, affecting the flame propagation process. Additionally, the water impedes the oscillation of the pressure waves, resulting in a generally flatter rate of pressure rise curve.

The typical monitoring curves from eight sensitive fire detectors, uniformly distributed along the pipeline in the natural gaswater layer explosion experiment, are presented in Fig. 9. The flame take-off time in the natural gas-water layer explosion experiment occurs earlier, and the explosive reaction is sustained within the range of 0.058—1.193 s, increasing the effective explosion duration by 110.19%. In this experiment, a faint, nearly transparent flame is observed slowly passing the observation window, and the phenomenon is extremely weak, accompanied by a subdued explosion sound.

It can be seen from the comparison of the pressure characteristic diagrams of the experimental results of the two sedimentary layers, both the water and diesel layers contribute to a reduction in the peak overpressure, though through different mechanisms. The water layer absorbs heat, dampening the pressure wave and reducing its intensity, while the diesel layer, through slower evaporation and combustion, releases energy more gradually, leading to a similar damping effect on the pressure wave. Thus, both layers play a role in lowering the peak overpressure.

In this experiment, the overall trend in flame brightness is observed to follow the order: natural gas-diesel layer > natural gas  $\gg$  natural gas-water layer. During the natural gas explosion experiment, as the explosion progressed, the time intervals between the flame's arrival at successive monitoring points increased, and the flame propagation velocity gradually decreased as it

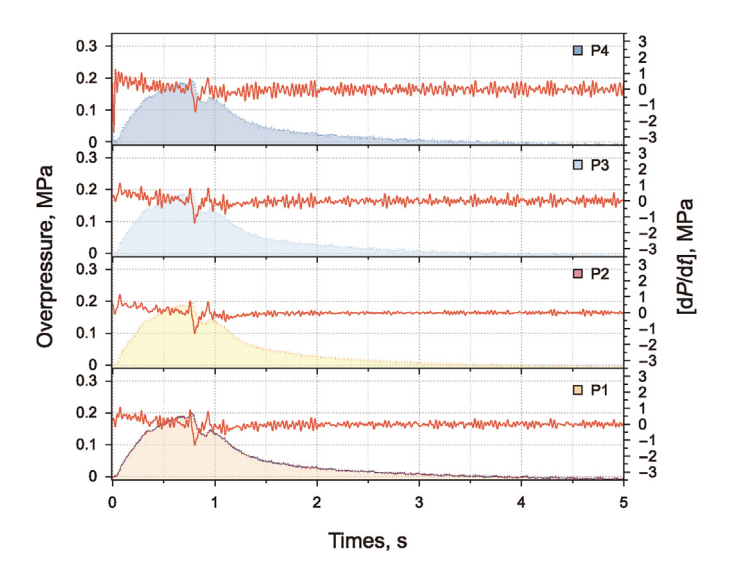
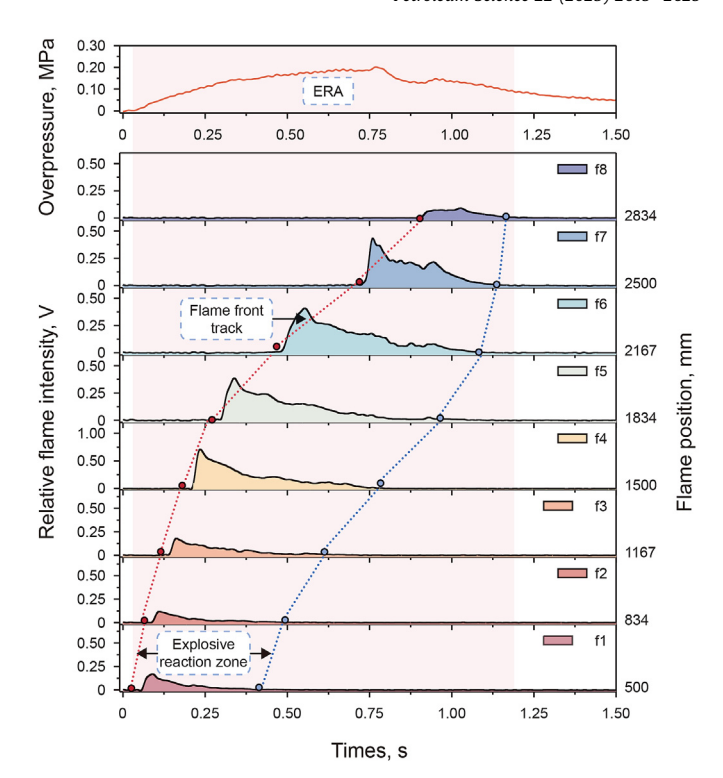


Fig. 8. Characteristics of gas explosion overpressure wave curves in an aquifer environment.



**Fig. 9.** Typical flame propagation and reaction zone characteristics of a gas explosion in an aquifer environment.

approached the end of the pipeline. After diesel was injected, the flame propagation velocity near the end of the pipeline increased. This occurred because the flame ignited the diesel during propagation, and the energy released from diesel combustion accelerated the flame's spread in the later sections of the pipeline. However, in the water-injected scene, the time intervals between flame arrivals at the monitoring points near the end of the pipeline became even larger, and the flame propagation velocity decreased more significantly compared to the natural gas explosion. This is due to water's higher specific heat capacity and surface tension (as shown in Table 3), which allow it to absorb heat from the flame and impede its spread. In both the water- and diesel-injected scenes, the explosion duration is significantly extended. This study attributes the prolonged duration in the water layer scene to the reduced flame propagation velocity toward the end of the pipeline, while in the diesel layer scene, the extended duration is attributed to the additional fuel provided by the diesel. Although the outcomes are similar, the underlying mechanisms differ.

# 3.2. Influence of liquid fullness degree on the propagation law of natural gas explosion

# 3.2.1. Mechanisms of diesel layer fullness degree on natural gas explosions

The comparison of explosion overpressure curves under different  $L_{\rm d}$  conditions in the natural gas-diesel layer explosion experiments is shown in Fig. 10. From this data, the peak

**Table 3**Specific heat capacity and surface tension of water/diesel at standard conditions.

Liquid	Specific heat capacity, J/kg·°C	Surface tension, mN/m
Water	4180	72.099
Diesel	2100	26.800

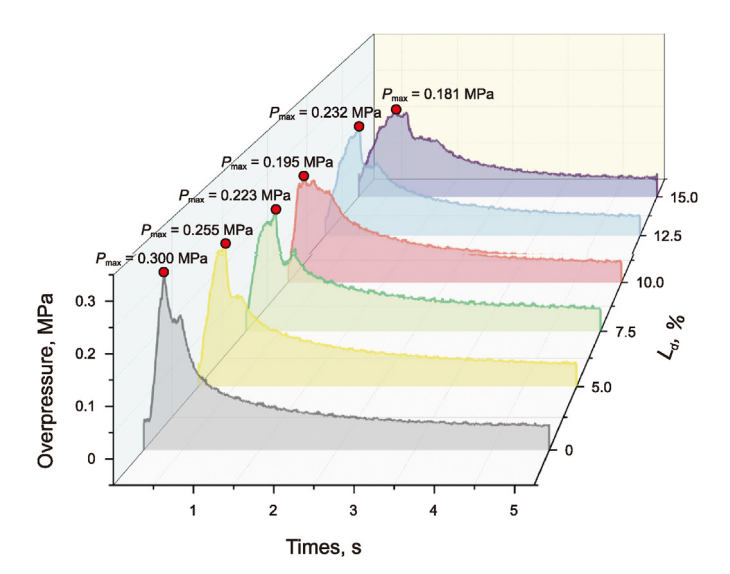


**Fig. 10.** Pressure characteristic curves of explosion at different diesel fullness degree (I, I)

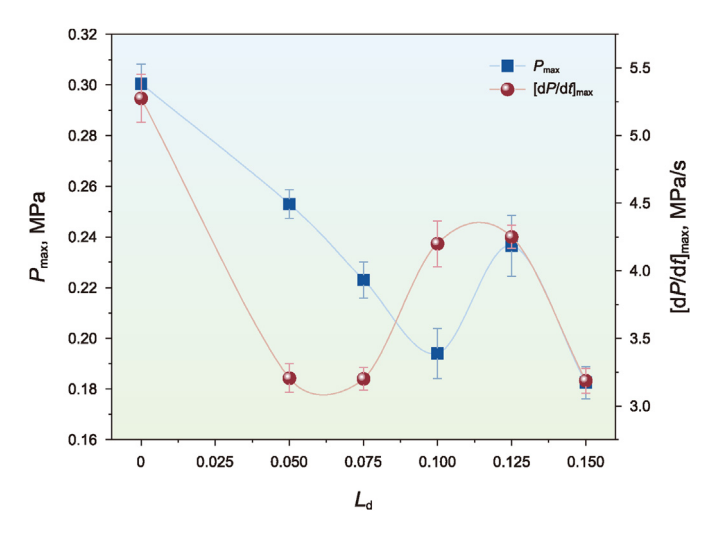


**Fig. 11.** Peak overpressure and maximum rate of pressure rise curves for explosions at different diesel fullness degree  $(L_d)$ .

overpressure  $P_{\rm max}$  and the maximum rate of pressure rise  $[{\rm d}P/{\rm d}t]_{\rm max}$  can be extracted, as illustrated in Fig. 11. It can be observed that as  $L_{\rm d}$  increases,  $P_{\rm max}$  and  $[{\rm d}P/{\rm d}t]_{\rm max}$  initially decrease, then increase, and subsequently decrease again. Furthermore, the  $P_{\rm max}$  and  $[{\rm d}P/{\rm d}t]_{\rm max}$  values in the diesel layer environment are lower than the peak overpressure of 0.3 MPa and the maximum rate of pressure rise of 5.3 MPa/s observed in the natural gas explosion experiment. This indicates that the liquid in the pipeline attenuates the oscillations of pressure waves. In the diesel environment,  $P_{\rm max}$  reaches a maximum value of approximately 0.255 MPa at a fullness degree of 5%, while  $[{\rm d}P/{\rm d}t]_{\rm max}$  peaks at around 4.25 MPa/s at a fullness degree of 12.5%. Notably,  $P_{\rm max}$  decreases by 23.5% when the fullness degree increases from 5% to 10%, then increases by 19% when it rises from 10% to 12.5%, and finally decreases by 21% when the fullness degree increases from 12.5% to 15%.

The comparison of flame front propagation velocities  $(S_d)$  in the natural gas-diesel layer explosion experiments along the pipeline is shown in Fig. 12. The flame propagation velocity curves exhibit a double-peak pattern under these conditions, which can be divided into four distinct regions. The first region, the acceleration zone (I),

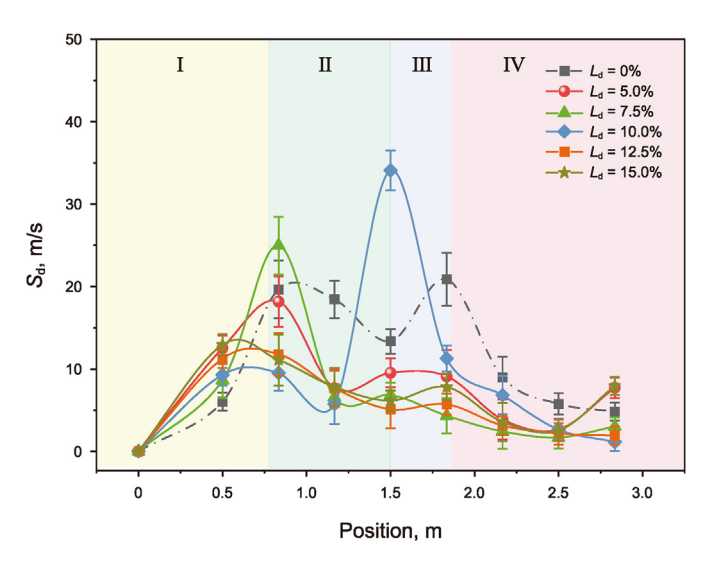


**Fig. 12.** Flame propagation velocity  $(S_d)$  for explosions at different diesel fullness degree  $(L_d)$ .

corresponds to the ignition of the natural gas-air mixture, where heat release accelerates the flame and drives the forwardpropagating pressure wave. The velocity of this wave approaches the local sound speed (approximately 340 m/s), significantly exceeding the flame velocity at this stage (less than 50 m/s). As a result, the pressure wave reflects off the closed section at the tail, while the flame front continues to propagate, leading to the deceleration zone (II). In this zone, the flame decelerates, and the pressure wave propagates in reverse until it reflects off the ignition surface, eventually catching up with and stretching the flame front, creating a secondary acceleration zone (III). Subsequently, the pressure wave gradually attenuates, but its compressive effect increases the pressure and concentration of unburned gas ahead of the flame front, causing the flame velocity  $(S_d)$  to decrease until it reaches the end of the pipeline. As the liquid fullness degree  $(L_d)$ increased from 5% to 10%, the peak flame propagation velocity (S<sub>d.</sub>  $_{\text{max}}$ ) increased from 18.17 m/s to 34.1 m/s. However, when  $L_{\text{d}}$  further increased to 15%,  $S_{d, max}$  decreased to 12.94 m/s, with the final flame propagation velocity under these conditions reaching 12.94 m/s. Under the current experimental conditions, the peak flame propagation velocity varies with different diesel deposition layer conditions, reaching a maximum of 34.1 m/s at  $L_{\rm d}=10\%$  and a minimum of 11.24 m/s at  $L_d = 12.5\%$ .

# 3.2.2. Mechanisms of water layer fullness degree on natural gas explosions

In the natural gas-water layer explosion experiments, a comparison of the explosion overpressure ( $P_{\rm max}$ ) curves for different  $L_{\rm w}$  values is shown in Fig. 13. The peak overpressure and the maximum rate of pressure rise ( $[{\rm d}P/{\rm d}t]_{\rm max}$ ) extracted from these curves are compared in Fig. 14. Both  $P_{\rm max}$  and  $[{\rm d}P/{\rm d}t]_{\rm max}$  in the natural gas-water layer experiments are lower than in the natural gas experiment.  $P_{\rm max}$  reaches a maximum of approximately 0.238 MPa at a 12.5% liquid fullness degree. Across different liquid fullness degrees,  $[{\rm d}P/{\rm d}t]_{\rm max}$  remains close to 2.1 MPa/s. Increasing the fullness from 5% to 10% results in a 21.9% decrease in  $P_{\rm max}$ . From 10% to 12.5%,  $P_{\rm max}$  increases by 51.6%, and from 12.5% to 15%, it decreases by 29.8%.

The comparison of the flame front propagation velocity  $(S_w)$  during natural gas-water layer explosion experiments along the pipeline is presented in Fig. 15. The velocity curve demonstrates a bimodal pattern. Additionally, the presence of water in the lower

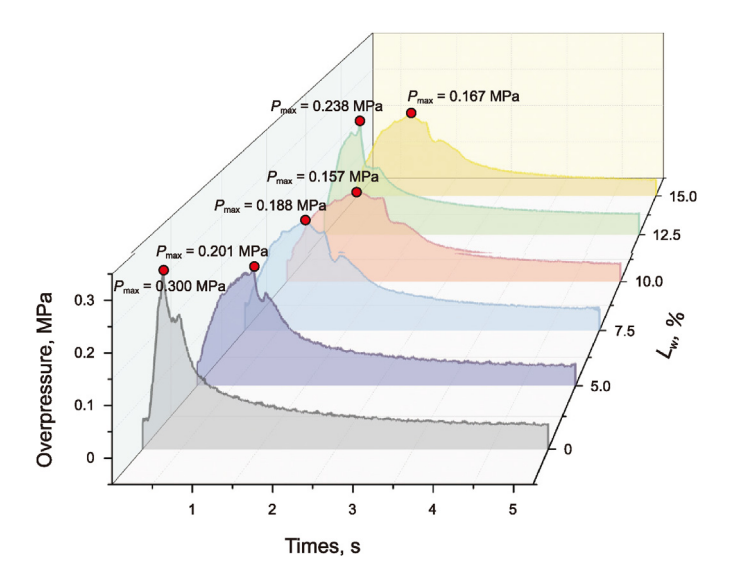


**Fig. 13.** Explosive pressure characteristic curves for different water layer fullness degree  $(I_m)$ 

section of the pipeline impedes flame propagation, leading to a reduced flame velocity in the acceleration zone I compared to the natural gas-only experiments. In secondary acceleration zone III, the flame velocity gradually increases. Subsequently, the pressure wave attenuates, but its compression effect increases both pressure and the concentration of unburned gas at the flame front. The flame velocity ( $S_{\rm w}$ ) then decreases as it propagates toward the end of the pipeline. Notably, as the water layer fullness ( $L_{\rm w}$ ) increases from 5% to 10%, the maximum flame velocity ( $S_{\rm w, max}$ ) decreases from 13.42 to 12.73 m/s. The addition of the water layer significantly reduces the flame velocity relative to the natural gas explosion experiments.

As shown in Fig. 15, the experimental error in this group is larger compared to other liquid layer experiments. This variability is likely due to experimental factors, particularly residual water vapor from previous explosions, which increased humidity and potentially slowed flame propagation. Despite extending the time interval between experiments to facilitate the evaporation of moisture, the residual water vapor may still have contributed to fluctuations in

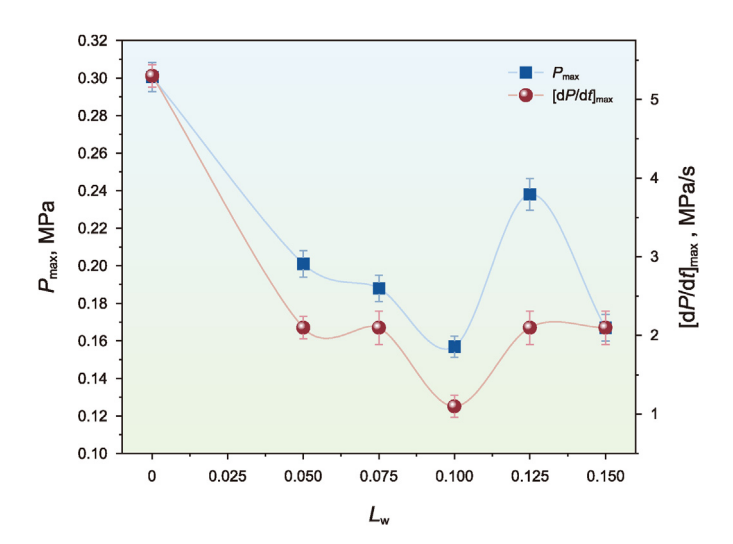


**Fig. 14.** Peak overpressure and maximum rate of pressure rise curves for explosions with different layer fullness degree  $(L_w)$ .

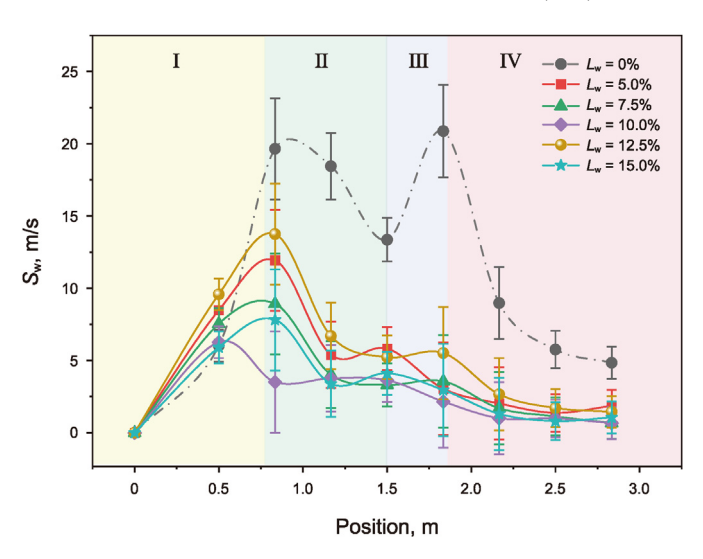


**Fig. 15.** Explosive flame propagation velocity  $(S_w)$  for different water layer fullness degree  $(L_w)$ .

the results. While the increased error introduces some volatility, the overall trend (i.e., the slowing effect of the water layer on the flame propagation velocity) remains evident.

As  $L_{\rm X}$  increases from 5% to 15%, the peak overpressure change curves for the natural gas-diesel layer and natural gas-water layer environments exhibit a similar trend. Specifically, when  $L_{\rm X}$  increases from 0% to 10%, the explosive reaction is primarily inhibited by the liquid environment, leading to a gradual reduction in peak overpressure. When  $L_{\rm X}$  reaches 12.5%, the liquid environment restricts the reaction space within the pipeline. Consequently, the length-to-diameter ratio of the pipeline increases from 27.5 to 34.8, resulting in greater inhibition of flame propagation velocity and pressure wave transfer. This enhances the intensity of the explosive reaction, causing an increase in both peak pressure and velocity peaks. However, as  $L_{\rm X}$  reaches 15%, the overall gas volume in the pipeline decreases while the liquid surface area increases, leading to an intensified inhibitory effect and a subsequent decrease in both peak pressure and flame propagation velocity peak.

In Fig. 16, the flame propagation velocity and flame images are compared for a change in  $L_x$  from 0% to 15%. In the initial stage, where  $L_w$  increases from 0% to 10%, the flame propagation velocity

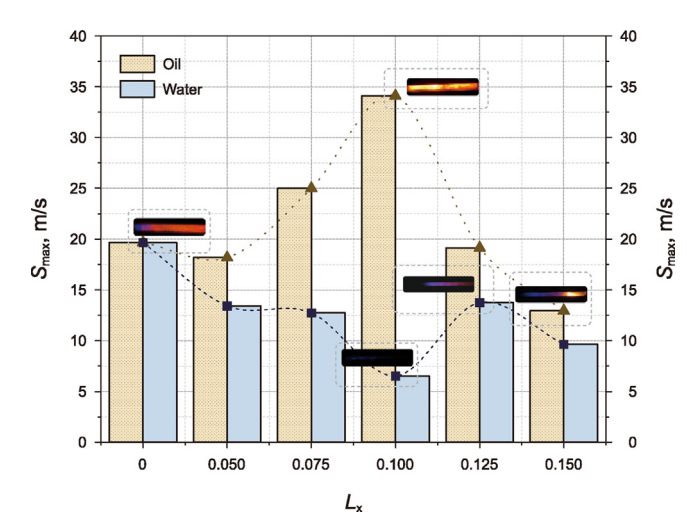


Fig. 16. Peak velocity of explosion flame propagation in different liquid environments.

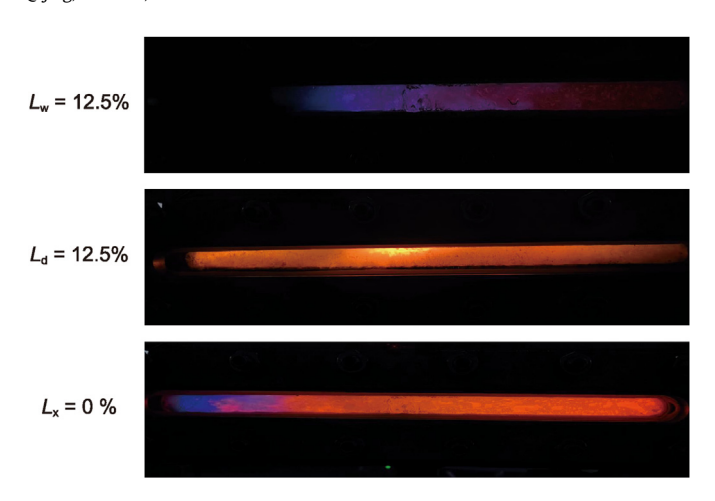


Fig. 17. Flame behavior under varying liquid deposition conditions.

 $(S_{\rm w})$  under water layer conditions decreases to 6.53 m/s, which is only 33.23% of the maximum velocity  $(S_{\rm max})$  of 19.65 m/s observed in the natural gas condition. As  $L_{\rm w}$  increases to 12.5%,  $S_{\rm w}$  rises to 13.75 m/s, though it remains below the maximum natural gas condition. In contrast, the flame propagation velocity  $(S_{\rm d})$  in the diesel layer shows a trend of first increasing and then decreasing with increasing  $L_{\rm d}$ . Specifically, as  $L_{\rm d}$  increases from 0% to 10%, the maximum flame propagation velocity in the diesel layer rises by approximately 73.5%, reaching 34.1 m/s. However, from  $L_{\rm d}=10\%-15\%$ , this maximum velocity decreases by 63.1%, resulting in comparable values for the diesel and water layers at their respective maximum velocities  $(S_{\rm max})$ .

As shown in Fig. 17, the flame front of a natural gas-air mixture with an equivalence ratio of 1.0 is blue-violet (temperature higher than 1500 °C), followed by a bright orange-red area (temperature around 1000–1200 °C), indicating that the explosive reaction extends beyond the flame front, with reactive gases in the product area continuing to participate in combustion. In the natural gas-diesel layer condition, the flame front is orange-red (temperature around 1000–1200 °C), followed by a bright white-gold oscillation in the flame (temperature around 1300–1400 °C), suggesting that the combustion of the diesel fuel enhances flame propagation. In contrast, under natural gas-water layer conditions, only a transparent flame sweeps through the product area, with the remaining

reactive mixture in the product area, indicating that the presence of water impedes the explosive reaction.

### 3.3. Explosive shock risk evaluation

### 3.3.1. Calculation of explosion energy

Using the prediction model (Wang et al., 2021) for blast wave energy ( $E_x$ ) in gas pipeline explosions, the blast wave energy of different liquid fullness degrees in water ( $E_w$ ) and diesel ( $E_d$ ) layer environments was calculated and converted to TNT equivalent values, as shown in Table 4. Under the experimental conditions, the maximum  $E_w$  is  $6.32 \times 10^6$  J, equivalent to 1.50 tons of TNT, while the maximum  $E_d$  is  $7.15 \times 10^6$  J, equivalent to 1.70 tons of TNT. These values are comparable to the damage caused by a 120 mm tank shell.

$$\begin{split} E_{\rm x} = & 1.3 \times 10^6 - 1.3 \times 10^6 e^{0.13R} + \left( -7.3 \times 10^6 + 6.4 \times 10^6 e^{0.17R} \right) \frac{\Delta P}{P_0} \\ & + \left[ -4.2 \times 10^5 + 2.5 \times 10^5 e^{0.37R} \right] \times \left( \frac{\Delta P}{P_0} \right)^2 \end{split} \tag{4}$$

where *R* is the distance from the ignition source, m;  $\frac{\Delta P}{P_0}$  is the differential pressure ratio.

The TNT equivalent of the blast wave energy is calculated by comparing the measured explosion energy with the energy released by a known mass of TNT. The formula used is: TNT equivalent (kg) = (Explosion energy/Energy of 1 kg TNT), where explosion energy is measured in joules, and the energy of 1 kg TNT is approximately  $4.184 \times 10^6$  J.

# 3.3.2. Determination of damage to underground space from blast impacts

Based on the explosive overpressure injury criterion in Table 5, the degree of damage caused by the explosion shock wave in each accident scene is assessed, as illustrated in Fig. 18. The results indicate that all experimental conditions of the explosion shock can cause damage to shockproof reinforced concrete. Notably, the peak overpressure in the diesel layer at  $L_{\rm d}=0\%$ , 5%, 7.5%, and 12.5%, as well as in the water layer at  $L_{\rm w}=12.5\%$ , is sufficient to destroy large-scale steel frame structures. The degree of explosive impact damage generally follows the trend: natural gas > natural gas-diesel layer > natural gas-water layer.

$$\begin{cases} (P - 0.342) \left( I - 1.494 \times 10^{-3} \right) = 3.74935 \times 10^{-4} (99\% \text{ lethality threshold}) \\ (P - 0.253) \left( I - 1.051 \times 10^{-3} \right) = 3.74935 \times 10^{-4} (50\% \text{ lethality threshold}) \\ (P - 0.73) \left( I - 0.258 \times 10^{-3} \right) = 3.74935 \times 10^{-4} (0\% \text{ lethality threshold}) \end{cases}$$
 (5)

**Table 4**Blast wave energy hazards.

$L_{\mathbf{x}}$	$E_{\rm w}$ , $ imes 10^6  m J$	TNT	$E_{\rm d}$ , $\times~10^6~{ m J}$	TNT
0	8.32	1.98	8.31	1.98
0.05	5.04	1.20	7.15	1.70
0.075	5.01	1.19	5.74	1.37
0.1	4.01	0.95	4.86	1.16
0.125	6.32	1.50	6.22	1.48
0.15	4.14	0.98	5.81	1.38

Based on overpressure guidelines for the fatality threshold and the Bowen overpressure-impulse injury threshold, the degree of injury caused by the experimental conditions was assessed. The results show that the peak overpressure in these experiments exceeded the fatality threshold for personnel. According to the Bowen Curve, when the diesel layer fullness degree ( $L_{\rm d}$ ) is greater than 5% and for all levels of water layer fullness ( $L_{\rm w}$ ), the shock effects from natural gas-air combustion result in a lethality rate

**Table 5** Explosive overpressure injury criterion (Wang et al., 2019).

Overpressure, MPa	Degree of building damage	Overpressure, MPa	Degree of bodily harm
0.006-0.015	Most of the glass on the pressure surface is broken	0.02-0.03	Minor damage
0.04-0.05	Large cracks in walls, falling roof tiles	0.03-0.05	Moderate impairment
0.07-0.1	Brick wall collapses	0.05-0.1	Serious injury
0.1-0.2	Anti-seismic reinforced concrete damage	>0.1	Death or fatal injury
0.2-0.3	Destruction of large steel frame structures		

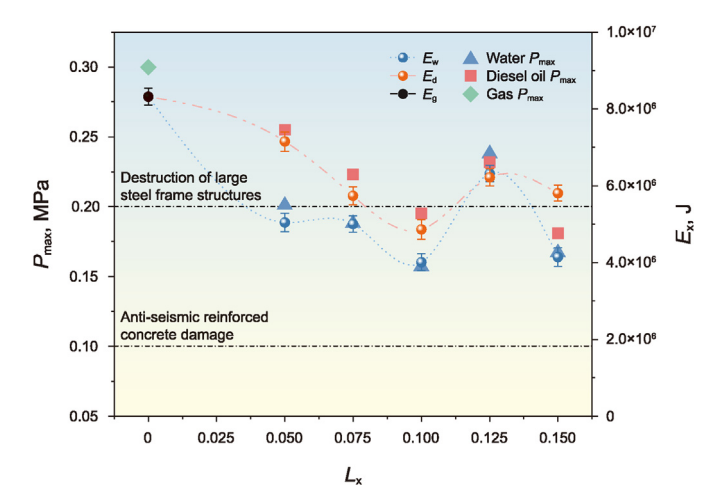
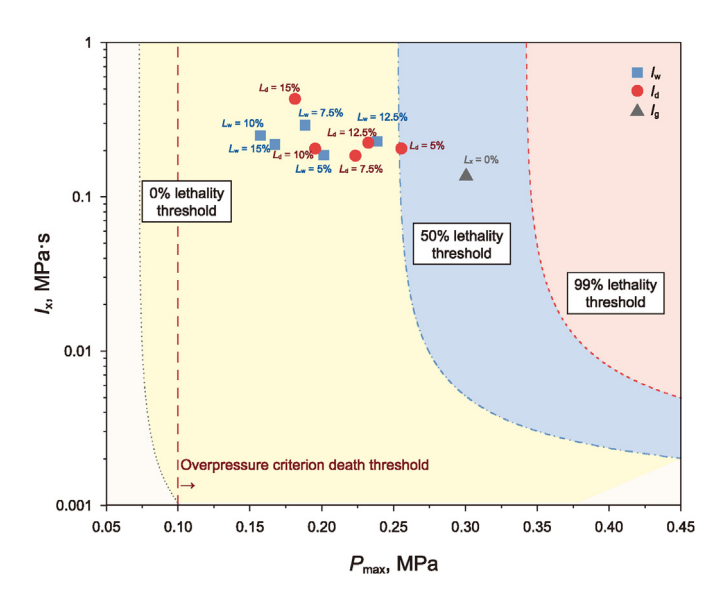


**Fig. 18.** Determination of damage to underground space structures by peak blast overpressure.



 $\textbf{Fig. 19.} \ \ \text{Hazardousness of the degree of human injury from the impact of a combustion explosion.}$ 

between 0 % and 50%. However, under conditions where the diesel layer fullness degree ( $L_{\rm d}$ ) is less than or equal to 5%, the shock effects from the explosion result in a personnel lethality rate between 50% and 99%.

It is illustrated in Fig. 19 that when a liquid deposition layer is present, both the peak overpressure and lethality decrease slightly. However, the peak overpressure remains higher than the critical threshold for fatality, and the lethality remains close to the 50% threshold. Additionally, due to the prolonged duration of the explosion, the impulse generated under liquid deposition conditions is higher than that in gas-only scenes. The maximum overpressure

impulse recorded under the experimental conditions is 0.43 MPa·s, occurring when the diesel fuel fullness is 15%.

#### 4. Conclusions

This study constructs a liquid-fillable horizontal natural gas explosion pipeline experimental system to investigate the propagation characteristics of natural gas explosions with liquid fullness ( $L_{\rm x}$ ) ranging from 5% to 15%. The effects of  $L_{\rm x}$  on explosion behavior in diesel and water layers are compared, and both blast energy and TNT equivalent are calculated. The main conclusions are as follows.

- (1) The peak explosion overpressure and pressure rise rate are significantly lower with the liquid layer compared to natural gas alone. In the diesel environment, P<sub>max</sub> is approximately 0.255 MPa at a 5% fullness degree. As the liquid fullness degree (L<sub>d</sub>) increases, the peak overpressure decreases, and the pressure rise rate increases. However, the heat absorption of the water layer dampens pressure wave oscillations, resulting in a relatively flat pressure rise curve without a distinct peak.
- (2) The explosion duration time increased by approximately 1x for both the water and diesel fuel layers. When both water and diesel fuel layers were present, the explosion duration was approximately doubled compared to the natural gasonly condition. The mechanisms differ: the evaporation combustion of the diesel layer prolongs the explosion duration, while the water layer reduces the flame propagation velocity. The maximum and minimum flame propagation velocities under the liquid deposition layer condition were 34.1 and 6.53 m/s, respectively.
- (3) In the water layer, the maximum blast wave energy  $(E_{\rm w})$  is  $6.32 \times 10^6$  J with a TNT equivalent of 1.50. In the diesel layer, the maximum blast wave energy  $(E_{\rm d})$  is  $7.15 \times 10^6$  J with a TNT equivalent of 1.70. The peak overpressure at diesel layer  $L_{\rm d}=0\%$ , 5%, 7.5 %, 12.5% and water layer  $L_{\rm w}=12.5\%$  is sufficient to damage large steel frame structures. The peak overpressure in all experimental conditions exceeded the critical value for personnel fatalities. Under natural gas and diesel layer conditions with  $L_{\rm d} \leq 5\%$ , the fatality rate due to the impact effect of the natural gas-air combustion explosion ranged from 50% to 99%.
- (4) The impulse from explosions with a liquid deposition layer is higher than that from natural gas-only experiments due to the longer explosion duration. Under experimental conditions, the maximum overpressure impulse was 0.43 MPa·s with a diesel fullness degree of 15%.

### **CRediT authorship contribution statement**

**Qi Jing:** Writing — original draft, Methodology, Formal analysis, Data curation, Laibin Zhang, Writing — review & editing, Investigation, Data curation. **Zi-Yu Fan:** Writing — review & editing, Supervision, Methodology, Conceptualization. **Rui Zhou:** Writing —

original draft. Yun-Tao Li: Methodology, Investigation.

### **Conflict of interest**

All authors disclosed no relevant relationships.

#### Acknowledgment

This article was supported by the National Natural Science Foundation of China (Project Approval Number: 52404270); Post-doctoral Innovative Talent Support Program (BX20230427); Post-doctoral Surface Fund Grants (2023M743874); Research Start-up Fund of China University of Petroleum (Beijing) (2462023XKBH017); Fundamental Research Project Grant of China Academy of Safety Science and Technology (2023JBKY07).

#### References

- Chen, C.H., Sheen, Y.N., Wang, H.Y., 2016. Case analysis of catastrophic underground pipeline gas explosion in Taiwan. Eng. Fail. Anal. 65, 39–47. https://doi.org/10.1016/j.engfailanal.2016.03.013.
- Feng, G.J., Zhang, J.L., Luan, G.W., Qiu, H.C., Bao, W., 2024. Research on diffusion characteristics of liquid jet effected by shock wave in supersonic high-enthalpy crossflow. Int. J. Heat Mass Tran. 222, 125181. https://doi.org/10.1016/ j.ijheatmasstransfer.2024.125181.
- Guo, P.K., Xu, C.Q., Lu, J.C., Wang, Z.R., Chang, X.Y., Hu, L., Wang, Z.P., Dong, J., Wang, W., 2024. Experimental study on propagation dynamics characteristic of premixed syngas/air explosion in parallel narrow channels. Fuel 363, 130866. https://doi.org/10.1016/j.fuel.2024.130866.
- He, Y.L., Fang, Q., Yuan, B.H., Cao, C.R., Zhan, Y.Y., Chen, X.F., Huang, C.Y., Zhang, Y.D., Ding, Q.Q., 2022. Explosion evolution behavior of methane/air premixed gas in a closed pipe filled with a bio-based porous material. Fuel 318, 123716. https://doi.org/10.1016/j.fuel.2022.123716.
- Lee, B., Wang, S.Y., Lin, T.C., Chang, H.H., 2021. Underground pipeline explosions and housing prices: quasi-experimental evidence from an urban city. Land Use Policy 111, 105782. https://doi.org/10.1016/j.landusepol.2021.105782.
- Li, Y.Z., Qian, X.M., Yuan, M.Q., Hou, L.F., Wu, Y.W., Duanmu, W.K., Chen, J., 2021. Quantitative evaluation of explosion consequences in urban underground drainage. Tunn. Undergr. Space Technol. 111, 103779. https://doi.org/10.1016/ itust.2020.103779
- Li, Y.Z., Qian, X.M., Zhang, S.Y., Sheng, J.J., Hou, L.F., Yuan, M.Q., 2023. Assessment of gas explosion risk in underground spaces adjacent to a gas pipeline. Tunn. Undergr. Space Technol. 131, 104785. https://doi.org/10.1016/j.tust.2022.104785.
- Lu, C., Guo, H., Li, M., Shao, X., Wang, J., Pan, R., 2024. The weakening and suppression effects of cavities on the propagation of gas explosions in pipes. J. Loss Prev. Process. Ind. 92, 105417. https://doi.org/10.1016/j.jlp.2024.105417.
- Lv, P.F., Ju, M.H., Zhang, J.X., Pang, L., Yang, K., Liu, K.Y., Shang, P.Y., 2021. Influence of water storage on deflagration characteristics of methane in confined. J. Loss Prev. Process. Ind. 73, 104600. https://doi.org/10.1016/j.jlp.2021.104600.
- Nowak, P.R., Szlachta, A., Gajewski, T., Peksa, P., Sielicki, P.W., 2023. Small-scale underwater explosion in shallow-water tank. Ocean. Eng. 288, 115894. https:// doi.org/10.1016/j.oceaneng.2023.115894.
- Pang, L., Li, W., Yang, K., 2025. Gas explosion overpressure loads in utility tunnels under different pipe support spacing. Tunn. Undergr. Space Technol. 155, 106193. https://doi.org/10.1016/j.tust.2024.106193.
- Qi, S., Li, Y.T., Zhou, S., Jing, Q., Zhang, L.B., Zhou, R., Chen, W.Y., Li, T., 2024. The premixed flame structure and combustion mechanism of clean hydrogen mixed

- with multi-component natural gas. Fuel 372, 132240. https://doi.org/10.1016/j.fuel.2024.132240.
- Shen, X.B., Dou, Z.G., Zhang, Z.W., Cong, B.H., Liu, H.F., Wang, F.C., 2022. Pressure dependence of combustion instability for premixed syngas/air in a closed channel. Int. J. Hydrogen Energy 47, 35171–35183. https://doi.org/10.1016/ j.ijhydene.2022.07.109.
- Sugiyama, Y., Tanaka, T., Matsuo, A., Homae, T., Wakabayashi, K., Matsumura, T., Nakayama, Y., 2016. Numerical simulation of blast wave mitigation achieved by water inside a subsurface magazine model. J. Loss Prev. Process. Ind. 43, 521–528. https://doi.org/10.1016/j.jlp.2016.07.015.
- Wang, D., Qian, X.M., Ji, T.C., Jing, Q., Zhang, Q., Yuan, M.Q., 2021. Flammability limit and explosion energy of methane in enclosed pipeline under multi-phase conditions. Energy 217, 119355. https://doi.org/10.1016/j.energy.2020.119355.
   Wang, K., Shi, T.T., He, Y.R., Li, M.Z., Qian, X.M., 2019. Case analysis and CFD nu-
- Wang, K., Shi, T.T., He, Y.R., Li, M.Z., Qian, X.M., 2019. Case analysis and CFD numerical study on gas explosion and damage processing caused by aging urban subsurface pipeline failures. Eng. Fail. Anal. 97, 201–219. https://doi.org/10.1016/j.engfailanal.2019.01.052.
- Xiao, H.H., Wang, Q.S., He, X.C., Sun, J.H., Yao, L.Y., 2010. Experimental and numerical study on premixed hydrogen/air flame propagation in a horizontal rectangular closed duct. Int. J. Hydrogen Energy 35, 1367—1376. https://doi.org/10.1016/ i.iihydene.2009.12.001.
- Xu, Y., Huang, Y.M., Ma, G.W., 2020. A review on effects of different factors on gas explosions in underground structures. Undergr. Space 5, 298–314. https:// doi.org/10.1016/j.undsp.2019.05.002.
- Yang, K., Li, W., Dai, X.L., Guo, Y.Y., Pang, L., 2024a. Effect of hydrogen ratio on leakage and explosion characteristics of hydrogen-blended natural gas in utility tunnels. Int. J. Hydrogen Energy 64, 132–147. https://doi.org/10.1016/ j.ijhydene.2024.03.247.
- Yang, K., Zheng, Z.R., Li, W., Shen, J., Lv, P.F., Pang, L., 2024b. Dynamic evolution of flame and overpressure of leakage and explosion of hydrogen-blended natural gas in utility tunnels. Int. J. Hydrogen Energy 96, 1–20. https://doi.org/10.1016/j.ijhydene.2024.11.290.
- Yang, W., Yang, X.F., Zhang, K., Liu, C.L., Zhang, Y.C., 2024c. Experimental study on the explosion flame propagation behavior of premixed CH<sub>4</sub>/H<sub>2</sub>/air mixtures with inert gas injection. Int. J. Hydrogen Energy 84, 106–117. https://doi.org/10.1016/j.ijhydene.2024.08.120.
- Yu, R.Z., Qiu, Y.Y., Xing, H.D., Xu, G.A., Wang, M.Y., Li, B., Xie, L.F., 2024. Experimental investigation on initiation mechanism, overpressure, and flame propagation characteristics of methane-air mixtures explosion induced by hexogen in a closed pipeline. Energy 288, 129746. https://doi.org/10.1016/j.energy.2023.129746.
- Zhang, Q., Fu, L.Y., Li, Z.Y., Fan, T., Ma, Y.L., Cai, P., Qian, X.M., Zhang, R.H., Chen, Y.Y., 2020. Coupling mechanism of natural gas deflagration flame and continuous water in closed pipeline. Process Saf. Environ. Prot. 143, 177–185. https://doi.org/10.1016/j.psep.2020.07.004.
- Zhang, C.B., Jin, P.G., Chen, C.F., Zhang, X., Zhou, Z.H., Geng, S., Zhang, Y., Lan, Y.H., Shi, X.Q., Cao, W.G., 2023. Flame propagation characteristics and surface functional groups changes of corn starch dust during the combustion process. Powder Technology 430, 118995. https://doi.org/10.1016/j.powtec.2023.118995.
- Zhao, H.Z., Lam, K.Y., Chong, O.Y., 2001. Water mitigation effects on the detonations in confined chamber and tunnel system. Shock Vib. 8, 349–355. https://doi.org/ 10.1155/2001/124019.
- Zhao, Y., Xiao, X., Zhang, X, Wang, B., Wu, C.S., Chu, Z.H., Shi, X.Q., Yu, Y.W., Zhao, H.X., Jiao, F.Y., Cao, W.G., 2024. Experiment study on the explosion suppressing characteristics and mechanism of melamine cyanurate and ammonium dihydrogen phosphate for lignite dust. Powder Technology 448, 120246. https://doi.org/10.1016/j.powtec.2024.120246.
- Zhou, G., Ma, Y., Kong, Y., Zhang, Q., Qian, X.M., Liu, Z.Y., Wang, K., Liu, Y., Yang, S.Q., Li, Y.Y., 2023. Influence of equivalence ratio and H<sub>2</sub> blended ratio on explosion propagation characteristics of DME/H<sub>2</sub> blended gas in closed narrow space. Int. J. Hydrogen Energy 48, 30132–30143. https://doi.org/10.1016/j.ijhydene.2023.04.101.